TASK QUARTERLY 6 No 2 (2002), 309–321

NUMERICAL SIMULATIONS OF AIR-POLLUTANTS IN WINDY ATMOSPHERE

JERZY K. MICHALCZYK[1] AND KRZYSZTOF MURAWSKI[2,1]

[1] *Department of Environmental Physics,*
Institute of Environmental Protection Engineering,
Technical University of Lublin,
Wapienna 40B, 20-618 Lublin, Poland
jerzyk@akropolis.pol.lublin.pl

[2] *Department of the Complex Physical Systems,*
Maria Curie-Skłodowska University,
Radziszewskiego 10, 20-031 Lublin, Poland
kmurawsk@tytan.umcs.lublin.pl

(Received 21 November 2001; revised manuscript received 10 January 2002)

Abstract: Spreading of gaseous pollutants in windy atmosphere is considered by means of numerical simulations of two-dimensional hydrodynamic equations. The parametric studies, which are performed for various magnitudes of a horizontal wind speed, reveal a plume development and a generation of vortices which occur as a result of Kelvin-Helmholtz instabilities. Mass density profiles exhibit high level of spatial and temporal variability. A spectral analysis of these profiles provides variable circular frequency and a wave number.

Keywords: environmental protection engineering, transport of air-pollutants, plume structure, turbulence

1. Introduction

Diffusion, convection and turbulence play a dominant role in transport of pollutants in the atmosphere of the Earth. These phenomena constitute basic mechanisms of the exchange of mass, momentum, and energy. As these processes are complex, it is justifiable to develop a simplified description of spatial spreading of the pollutants. A parameterization of these processes must be applied, *i.e.* elementary physical factors ought to be distinguished. By means of these factors, the state of medium – in this case the atmospheric air – will be described. Moreover, one has to formulate relationships between various factors and their magnitudes, such as spatial distribution of the pollutants and profiles of the wind velocity, air temperature, and intensity of mixing. These relationships can be found on the basis of theoretical and experimental considerations.

As a monitoring network must be established and maintained, the experimental research of the Earth's atmosphere is expensive. The results which can be obtained in this way usually refer to a limited set of spatial points and parameters. It is also impossible to separate all factors that exert an influence on conditions of measurements. As a consequence of that, it is very difficult to make a correct analysis of these results. Besides, the results obtained in the monitoring stations provide only an image of the event which already took place, and as such they show effects of these events only. On the other hand, laboratory experiments allow us to investigate various factors. Unfortunately, their differentiation is often constrained by insufficient technical abilities.

Meanwhile, as computer techniques have been developed and computing power in both speed and storage increases, mathematical modeling of real physical phenomena acquires more and more significance. Each model is characterized by a mathematical structure, time-, and spatial-scales, as well as by a type and a number of introduced data. The state of the atmosphere and parameters of emission are given then by characteristic coefficients which can be determined experimentally. This kind of approach refers to statistical models and to models that are based on a Gauss' equation or a differential Pasquill's equation [1]. Computer simulations consist of numerical solutions of mathematical equations that describe both spreading and transformation of particles or certain volumes of fluids. The world literature presents an abundance of models which within certain limits reveal a good agreement with experiments, *e.g.* [1–6].

Mathematical modeling possesses many advantages. It can assess the existing state of the air-pollution, simulate the effect of future emission concentrations as well as predict a risk due to fatal emissions. Numerical modeling is expected to provide accurate data for urban and country planning, location of future emission centers and design of protected zones.

Recently, two-dimensional numerical simulations of continuous emission of one-component gas into the gravitationally stratified, isothermal and static atmosphere were performed by Michalczyk *et al.* [4, 7, 8]. It is natural now to analyze the spatial distribution of pollutants that are transported by wind. In the simplest conceivable model a wind velocity vector is horizontal and time-independent. However, two different vertical profiles are considered. The first profile corresponds to a height-independent velocity. In another profile the wind velocity grows linearly with height. Having determined the wind profile, we adapt a modern numerical code that solves a set of hydrodynamic equations which describe the dynamics of the pollutants and the ambient air. This model is expected to give more adequate results than other models which are based on a single advection equation, *e.g.* [6].

The paper is organized as follows. A model of the atmosphere is presented briefly in Section 2. A numerical model and the numerical code are described in Section 3. Section 4 presents a discussion of the numerical results. This paper is concluded by a short summary of the main results.

2. Mathematical model

The dynamics of air-pollutants can be described by the hydrodynamic equations:

$$\frac{\partial \rho}{\partial t} + \nabla \cdot (\rho \mathbf{V}) = S_\rho + S_D, \tag{1}$$

$$\frac{\partial (\rho \mathbf{V})}{\partial t} + [(\rho \mathbf{V} \cdot \nabla)\mathbf{V}] = -\nabla p + \rho \mathbf{g} + \mathbf{S_V}, \tag{2}$$

$$\frac{\partial E}{\partial t} + \nabla \cdot (E\mathbf{V}) = -\nabla \cdot (p\mathbf{V}) + S_E \tag{3}$$

which reveal three physical principles, namely: the mass is conserved, 2nd Newton's law is fulfilled, and the energy is conserved. In Equations (1)–(3) ρ is the mass density, $\mathbf{V}$ is the velocity, $\mathbf{g}$ is the gravitational acceleration, t denotes time, p stands for the gas pressure, and $E = \frac{p}{\gamma - 1} + \frac{\rho V^2}{2}$ is the total (internal and kinetic) energy density, where $\gamma = \frac{c_p}{c_V} = 1.4$ is the adiabatic constant that is expressed by the ratio of specific heats c_p and c_V. The x-axis lies in the horizontal direction and y denotes vertical coordinate. In our model we assumed inviscid flow by dropping the viscous terms in the general set of the hydrodynamic equations. These viscous terms are negligibly small for large spatial scales which we want to study. Henceforth, we limit our discussion to a two-dimensional case with $\frac{\partial}{\partial z} = 0$.

In Equation (1), S_D is a diffusive term such that:

$$S_D = \nabla \cdot [D(x,y,t,\rho) \nabla \rho(x,y,t)]. \tag{4}$$

In the real atmosphere this diffusion is referred to as molecular diffusion. Assuming that the diffusive coefficient D is a constant, the latter equation can be rewritten as:

$$S_D = D \nabla^2 \rho.$$

The quantities S_ρ, $\mathbf{S_V}$ and S_E denote the source terms which are associated with the emission of pollutants. If the emittor of its width x_0 is placed at the height $y = y_0$, the emission that takes place for $y > y_0$ can be realized as follows:

$$\rho_e = \rho_{e0} e^{-\frac{y - y_0}{x_0}}, \quad V_{ey} = \text{const}. \tag{5}$$

As a consequence of that the source term S_ρ is:

$$S_\rho = \begin{cases} \frac{\dot{E}}{A \cdot x_0} e^{-\frac{y - y_0}{x_0}}, & y \geq y_0, \\ 0, & y < y_0, \end{cases} \tag{6}$$

where $\dot{E} = \rho_{e0} V_{ey} A$ is the flux of the pollutants that are emitted from the area A, ρ_{e0} and V_{ey} are density and velocity of the pollutants, respectively, and x_0 is a spatial unit. The remaining source terms $\mathbf{S_V}$ and S_E are given by the following expressions:

$$\mathbf{S_V} = S_\rho V_{ey} \hat{\mathbf{y}}, \tag{7}$$

$$S_E = \frac{p_e}{\gamma - 1} \frac{V_{ey}}{x_0} - \frac{1}{2} V^2 (S_\rho + S_D) + \mathbf{V} \cdot \mathbf{S_V} - \rho \mathbf{V} \cdot \mathbf{g}. \tag{8}$$

The source term S_ρ that is given by Equation (6) acts above the emittor only. There is no emission below and at both sides of the smokestack and S_ρ equals zero there. In this paper it is assumed that the emission is time-independent and as a consequence of that S_ρ does not depend on t.

3. Numerical model

3.1. Numerical code

Our approach is based on a use of the CLAWPACK (Conservation LAWs PACKage) code which is a collection of Fortran routines for solving a hyperbolic system of conservation laws. The general structure of the code is described in details in the user notes by LeVeque [9].

For the numerical purposes, the hydrodynamics Equations (1)–(3) are written in the conservative form:

$$\frac{\partial}{\partial t}\mathbf{u}+\frac{\partial}{\partial x}\mathbf{f}+\frac{\partial}{\partial y}\mathbf{g}=\mathbf{S}, \tag{9}$$

where $\mathbf{S}$ and $\mathbf{u}$ denote the source vector and the state vector, respectively, such that:

$$\mathbf{u}=[\rho,\rho V_x,\rho V_y,E]^T. \tag{10}$$

The symbols $\mathbf{f}$ and $\mathbf{g}$ are the vector fluxes: $\mathbf{f}=\left[\rho V_x,\rho V_x^2+p,\rho V_x V_y,EV_x\right]^T$ and $\mathbf{g}=\left[\rho V_y,\rho V_x V_y,\rho V_y^2+p,EV_y\right]^T$.

The CLAWPACK code uses a wave propagation method [10, 11]. Additionally, a Riemann solver is adapted. The Riemann solver decomposes data at cell edges into a set of waves and wave speeds. The most famous Riemann solver is due to Roe [12]. To suppress numerically induced oscillations, flux limiters are used.

Problems with source terms $\mathbf{S}(\mathbf{u})$ are generally solved using the Godunov splitting in which the solution of the homogeneous equation, $\frac{\partial}{\partial t}\mathbf{u}+\frac{\partial}{\partial x}\mathbf{f}+\frac{\partial}{\partial y}\mathbf{g}=0$, is alternated with solutions of the equation $\frac{\partial}{\partial t}\mathbf{u}=\mathbf{S}(\mathbf{u})$. An exception is the gravity source term that is treated by the Godunov splitting method, developed by LeVeque [13]. This method is essentially based on implementation of a Riemann problem at the center of each grid cell whose flux difference exactly cancels the source term. Such approach has no problem with preserving steady states and it accurately calculates small perturbations of such states.

The method used here is a finite-volume method on a uniform rectangular grid Δx, Δy. In two dimensions Equation (9) can be discretized as follows:

$$\mathbf{U}_{i,j}^{n+1}=\mathbf{U}_{i,j}^{n}-\Delta t\left[\frac{1}{\Delta x}\left(\mathbf{F}_{i+\frac{1}{2},j}-\mathbf{F}_{i-\frac{1}{2},j}\right)+\frac{1}{\Delta y}\left(\mathbf{G}_{i,j+\frac{1}{2}}-\mathbf{G}_{i,j-\frac{1}{2}}\right)\right], \tag{11}$$

where $\mathbf{U}_{i,j}^{n}$ is an average of $\mathbf{u}(x=i\cdot\Delta x,y=j\cdot\Delta y,t=n\cdot\Delta t)$ over the numerical cell (i,j), $\mathbf{F}$ and $\mathbf{G}$ are fluxes that are evaluated at cell interfaces. The waves arising from a solution of Equation (11) are then used to define second-order correction terms. A transverse splitting of the waves is also performed to improve stability and resolution.

We have adapted this code by setting initial and boundary conditions as well as introduced a procedure for numerical realization of emission and diffusion.

3.2. Initial and boundary conditions

Initially, at $t=0$, the density ρ_0 and pressure p_0 correspond to the isothermal atmosphere of its temperature $T_0=293\mathrm{K}$ such as:

$$\begin{aligned}\rho_0(y)&=\frac{p_{00}}{gh_p}e^{-\frac{y}{h_p}},\\ p_0(y)&=p_{00}e^{-\frac{y}{h_p}}.\end{aligned} \tag{12}$$

They are drawn schematically in Figure 1. In the latter equations $p_{00} = 1013.25\,\mathrm{hPa}$ is the ground ($y = 0$) pressure with the mass density $\rho_{00} = 1.29\,\mathrm{kg/m^3}$, and $h_p = 8077\,\mathrm{m}$ represents an altitude at which the pressure decreases e times. These values provide the sound speed $c_s = 333\,\mathrm{m/s}$.

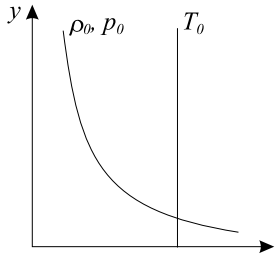

Figure 1. Equilibrium profiles of the mass density ρ_0, pressure p_0, and temperature T_0 for the case of the isothermal atmosphere

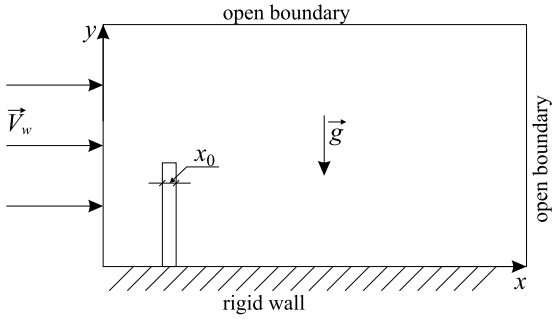

Figure 2. Numerical box and geometry of the system

The simulation box is given by $-15x_0 \le x \le x_{max}$ and $0 \le y \le y_{max}$, where x_0 is the width of the emittor (Figure 2). We assume that the height of the emittor is $25x_0$. The left boundary is the inflow boundary which is set by specification of the wind mass density $\rho_w = \rho_0$ and the wind speed V_w at $x = -15x_0$. The bottom boundary ($y = 0$) corresponds to a rigid wall with $V_y(x, y = 0) = 0$. So, a signal does not cross this boundary. This condition is not important for light pollution which is convected upwards and do not reach the bottom boundary. As a consequence of that, we neglected roughness of the ground.

The top ($y = y_{max}$) and right boundaries ($x = x_{max}$) are in the present model entirely open. So, any signal can easily leave the simulation area. The location of these two boundaries varies in dependence on the wind speed (Table 1). The computational area is divided into an uniform grid with the number of points which are adjusted to a wind speed (Table 1).

The emission is realized by specifying the source terms which are given by Equations (6)–(8). In the present simulations the mass density ρ_e, the emission velocity V_{ey} and the temperature T_e of the emitted pollutants are set constant such that: $\rho_e = 0.1\rho_{00}$, $V_{ey} = 15\,\mathrm{m/s}$, and $T_e - T_n = 5(T_0 - T_n)$, where T_n is normal temperature of the air, *viz.* 273 K.

In the case of y-independent wind speed we performed a number of numerical runs with various wind speeds, *i.e.*: (a) $V_w = 2.5\,\mathrm{m/s}$, (b) $V_w = 5\,\mathrm{m/s}$, (c) $V_w = 7.5\,\mathrm{m/s}$, (d) $V_w = 10\,\mathrm{m/s}$, and (e) $V_w = 15\,\mathrm{m/s}$ (see Table 1). The influence of constant diffusion with $D = 0.2\,\mathrm{cm}^2/\mathrm{s}$ is analysed in two cases, *i.e.*: (f) $V_w = 2.5\,\mathrm{m/s}$, and (g) $V_w = 10\,\mathrm{m/s}$.

Table 1. Parameters for numerical runs (a)–(i)

	Cases	Wind speed	Number of cells along direction		Actual distance covered along direction	
		V_w [m/s]	x	y	x [m]	y [m]
Diffusion-free cases, $D = 0$	(a)	2.5	160	160	80	80
	(b)	5.0	240	160	120	80
	(c)	7.5	400	160	200	80
	(d)	10	500	120	250	60
	(e)	15	500	120	250	60
Diffusive cases, $D \neq 0$	(f)	2.5	160	160	80	80
	(g)	10	500	120	250	60
Linear wind profile	(h)	$5 \rightarrow 7.5$	300	160	150	80
	(i)	$10 \rightarrow 15$	500	120	250	60

Furthermore, we performed numerical simulations for the wind speed that grows linearly with height in such a way that at $y = 100x_0$ the wind speed is $\frac{3}{2}$ times higher than the wind speed at the ground ($y = 0$), *i.e.* $V_w(y = 100x_0) = \frac{3}{2}V_w(y = 0)$. These two cases are denoted by (h) $V_w = 5 \rightarrow 7.5\,\mathrm{m/s}$ and (i) $V_w = 10 \rightarrow 15\,\mathrm{m/s}$ in Table 1.

4. Numerical results

4.1. Constant wind speed

In this part of the paper we consider the case of y-independent wind speed, $V_w \neq V_w(y)$.

Figure 3 displays spatial mass density profiles at time $t = 15\,\mathrm{s}$ which corresponds to quasi-stationary state. The wind speed V_w is chosen equal $2.5\,\mathrm{m/s}$. The diffusion-free ($D = 0$) and diffusive ($D = 0.2\,\mathrm{cm}^2/\mathrm{s}$) cases are denoted respectively by (a) and (f) in Table 1 and are shown in Figure 3, bottom left and right panels, respectively. For comparison purposes the top panel of Figure 3 shows the case of static ($V_w = 0$) atmosphere. Development of a plume and vortices is clearly seen here. This plume is convected upwards as a result of the buoyancy force. The vortices are a consequence of the Kelvin-Helmholtz instabilities which result from a velocity gradient. A spatial distribution of pollution is considerably affected by the wind which entirely alters the initially vertical direction of the emission (bottom left panel of Figure 3). A number of clouds that exhibit various spatial scales are characteristic for mild wind. The vortices, which occur at the border between the plume and the ambient air, penetrate a region far away from the emittor. The effect of diffusion is to enhance a vertical spreading of pollutants as well as restructure the flows far away from the emittor (bottom right panel of Figure 3).

Figure 4 displays the results for various values of the wind speed: $V_w = 5\,\mathrm{m/s}$ (top), $V_w = 10\,\mathrm{m/s}$ (middle), and $V_w = 15\,\mathrm{m/s}$ (bottom), respectively. A comparison

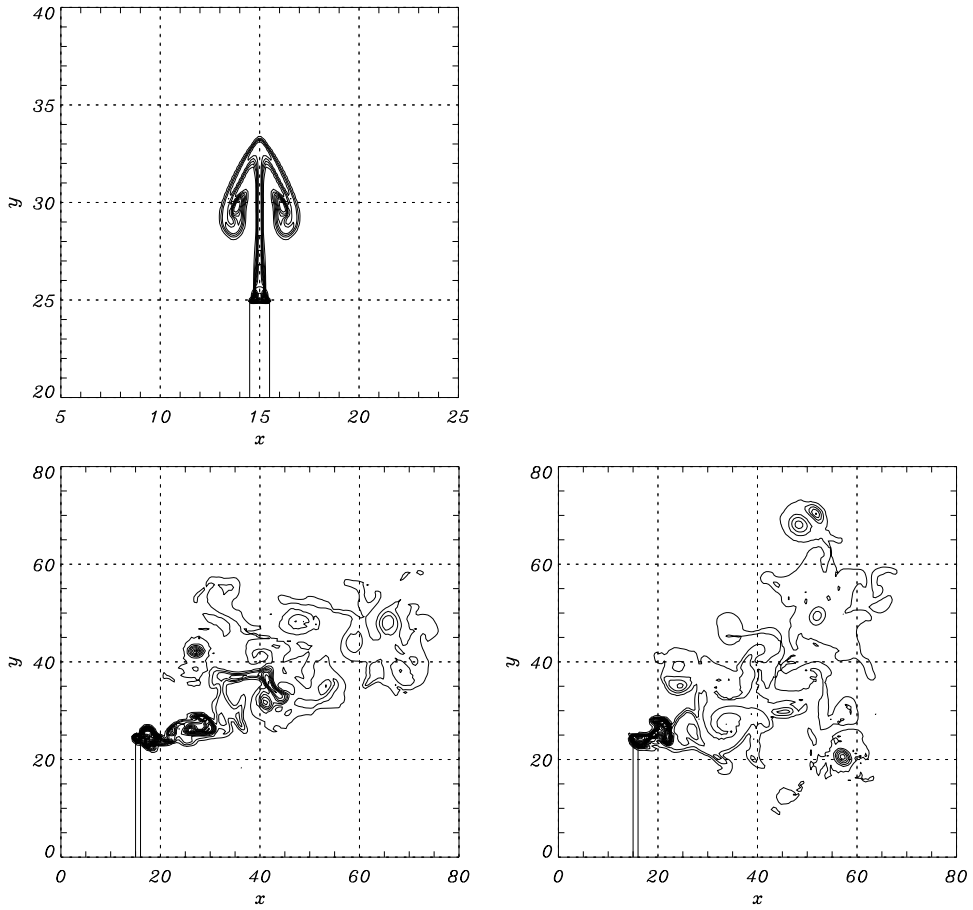

Figure 3. Spatial mass density profiles in the case of static ($V_w = 0$) atmosphere (top) as well as diffusion-free (bottom left panel) and diffusive (bottom right panel) cases for the wind speed $V_w = 2.5\,\mathrm{m/s}$

of these figures leads to a conclusion, that the wind speed influences both the vertical spreading of the plume and the distance which is covered by the pollutants. For stronger wind a plume can be transmitted farther away from the emittor and it is more collimated (the plume extends less in the vertical direction).

The mass density decreases with the distance down from the emittor and the clouds of pollution are formed. A distance at which separate clouds begin to be formed, grows with wind strength. It is higher than 50 m (Figure 4, top), 150 m (Figure 4, middle), and 250 m (Figure 4, bottom) in the case of the wind speed 5 m/s, 10 m/s, and 15 m/s, respectively. These clouds are accompanied by small vortices (*e.g.*, $x = 110x_0$ and $y = 65x_0$ in Figure 4, top).

The results for $V_w = 10\,\mathrm{m/s}$ and $V_w = 15\,\mathrm{m/s}$ reveal clouds of pollution which develop along the outskirts of the plume. These clouds originate from the Kelvin-Helmholtz (KH) instabilities which lead to a presence of vortices. A growth rate $\Gamma = \mathrm{Im}(\omega)$ of the KH instabilities can be estimated as (*e.g.* [14]):

$$\Gamma^2 = \frac{\rho_0 \cdot (\rho_0 + \rho_e)}{[\rho_0 + (\rho_0 + \rho_e)]^2} [k \cdot (V_e - V_0)]^2, \tag{13}$$

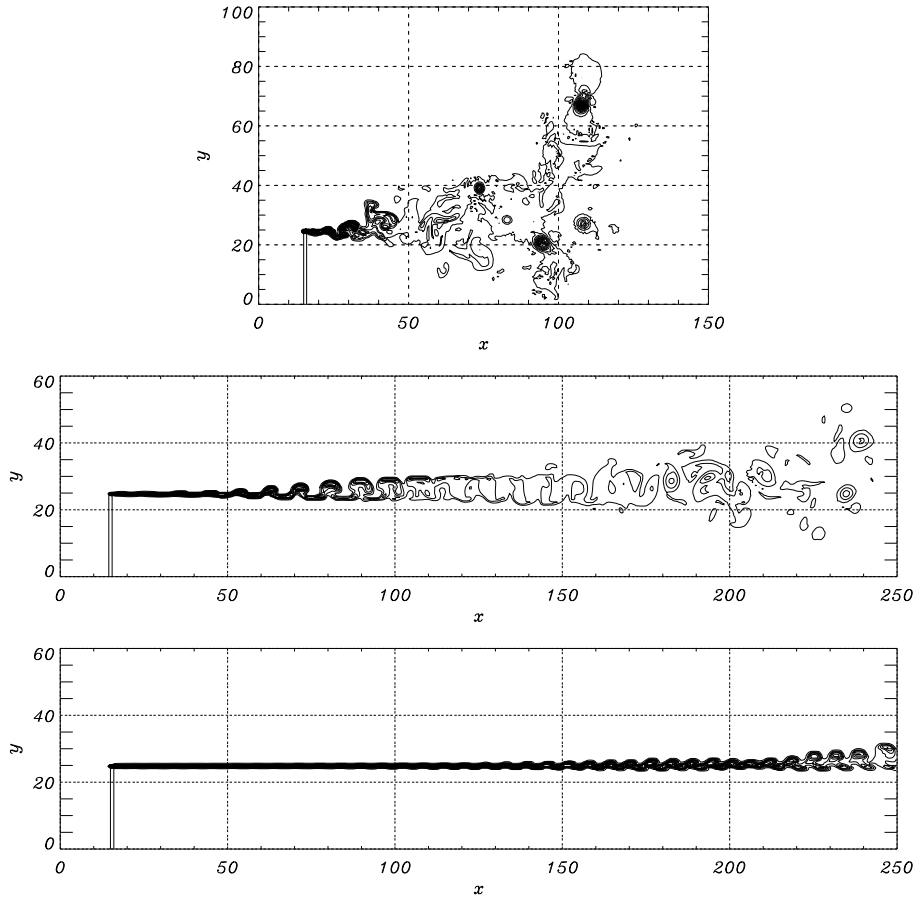

Figure 4. Spatial mass density profiles for the wind speeds $V_w = 5\,\mathrm{m/s}$ (top), $V_w = 10\,\mathrm{m/s}$ (middle), and $V_w = 15\,\mathrm{m/s}$ (bottom)

where ρ_e, ρ_0, $\vec{V}_e$ and $\vec{V}_0$ are the mass densities and velocities of the pollution and the ambient air, respectively. The wave number k of the wave with its length λ is represented by $k = 2\pi/\lambda$, and $\omega = 2\pi/T$ is the circular frequency of the wave. The period T corresponds to the time of appearance of the following concentrated clouds. If we assume that the distance between the centers of the neighbouring clouds is equal to the wavelength λ, then the period T for $V_w = 10\,\mathrm{m/s}$ (Figure 4, middle) can be estimated from Equation (13) as equal 4 s, in agreement with the numerical results.

In the case of the wind speed V_w equals to the emission speed V_{ey}, *i.e.* $V_w = V_{ey} = 15\,\mathrm{m/s}$ (Figure 4, bottom), a straight horizontal plume is developed. This plume is hardly altered in the region $x < 100x_0$, where it is bounded from above and below by the streams of the air. In the region $x > 100x_0$ the plume topology is altered by the presence of vortices. As a result of buoyancy force the plume is shifted upwards. At $x = 250x_0$ its center is at $y > 25x_0$.

For the wind speed $V_w = 10\,\mathrm{m/s}$ we simulated the case of the diffusion $D = 0.2\,\mathrm{cm}^2/\mathrm{s}$ (not shown). A comparison of this case to the diffusion-free case (Figure 4, middle) leads to a conclusion that in the case of a high wind speed the effect of diffusion is negligibly small.

4.2. Linear wind profile

We consider here the case of the wind speed which grows linearly with the height y. We assume that the wind speed at the altitude $y = 100x_0$, $V_w(y = 100x_0)$, is 50% higher than the speed at the ground, $V_w(y = 0)$. Specifically, we consider the case of $V_w(y = 0) = 10\,\mathrm{m/s}$, then $V_w(y = 100x_0) = 15\,\mathrm{m/s}$. This case is presented in Figure 5, which reveals a general structure of the plume. The ripples occur in the region $x > 90x_0$. They are more developed than in Figure 4, middle panel. As a consequence of the linear wind profile these ripples are asymmetric, *i.e.* the top ripples are more pronounced than the bottom ones. In this case an action of the buoyancy force is also more apparent because the plume is shifted up more than in Figure 4, middle panel.

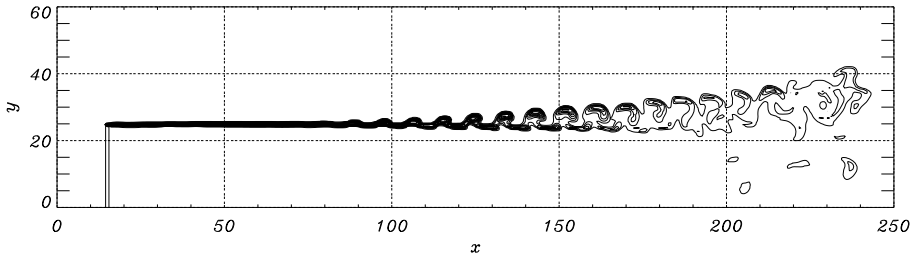

Figure 5. Spatial mass density profile for the linear wind speed with $V_w(y = 0) = 10\,\mathrm{m/s}$

4.3. Wave motion

In this part of the paper we present the results of spectral analyses of the mass density profiles. These analyses lead to the wave number k and the circular frequency ω. Thereby, we will characterize the wavy character of the spreading of the pollution in the atmosphere.

In the simulation area, at the altitude that is equal to the height of the emittor, *i.e.* $y_e = 25x_0$, we place four detectors at $x_1 = 50x_0$, $x_2 = 100x_0$, $x_3 = 150x_0$, and $x_4 = 200x_0$. These detectors collect the mass density as a function of time, $\rho = \rho(x_n, y = y_e, t)$, $n = 1,2,3,4$. A typical mass density profile is presented in Figure 6 which reveals oscillations.

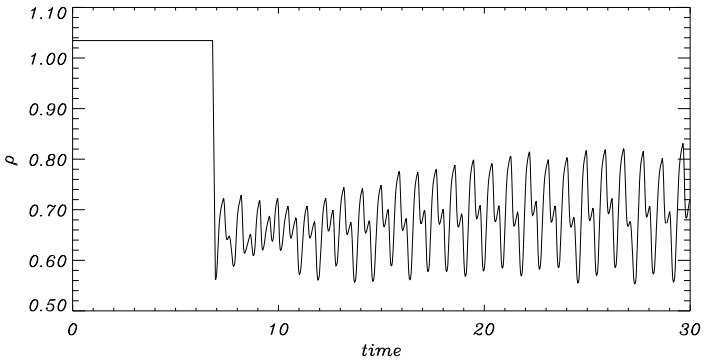

Figure 6. Time signature of a signal which is collected at the height $y = 25x_0$ and the horizontal position $x_1 = 50x_0$. The wind speed V_w is y-independent and equals 10 m/s

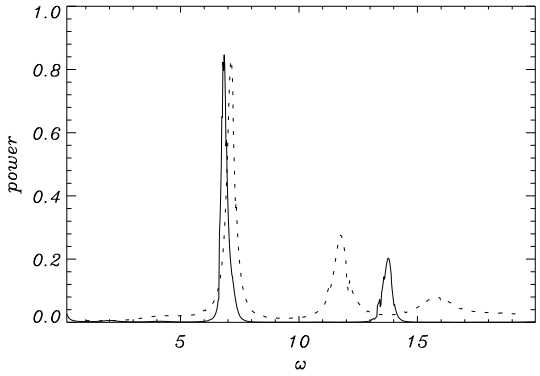

Figure 7. Frequency spectra for the time profiles collected at $x_1 = 50x_0$ (Figure 6) – solid line, and $x_2 = 150x_0$ (not shown) – dotted line

A spectral analysis of this profile leads to the frequency spectra which are shown in Figure 7.

Two different spectral lines are located at $\omega_1 \cong 7\,\mathrm{Hz}$ and $\omega_2 \cong 14\,\mathrm{Hz}$. The latter frequency occurs as a result of quadratic nonlinearity which generates frequencies at $\omega_n = n\omega_1$, $n = 2,3,\ldots$ [15].

A detailed description of a frequency shift is presented in Figure 8 which illustrates the frequency as a function of the distance x.

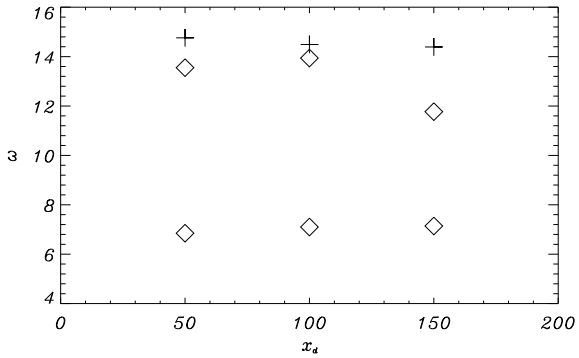

Figure 8. The frequency of oscillations as a function of the distance x from the emittor. The crosses and diamonds correspond to $V_w = 15\,\mathrm{m/s}$ and $V_w = 10\,\mathrm{m/s}$, respectively

It is noteworthy that for $V_w = 10\,\mathrm{m/s}$ the frequency $\omega_1 \cong 7\,\mathrm{Hz}$ is shifted towards the higher frequency with the distance from the emittor. In the case of $V_w = 15\,\mathrm{m/s}$ the basic frequency $\omega_1 \cong 7\,\mathrm{Hz}$ is reduced with the distance. The spectral line at $\omega_2 \cong 30\,\mathrm{Hz}$ is very weak and therefore it is not taken into consideration in our study. Note that for the strong wind of $V_w = 15\,\mathrm{m/s}$ the basic frequency $\omega_1 \cong 15\,\mathrm{Hz}$ (represented by crosses) decreases slightly with x. The signal associated with ω_2 is very weak and this frequency is not presented in Figure 8. However, it exhibits the same tendency as ω_1. The weaker wind of $V_w = 10\,\mathrm{m/s}$ leads to an increase (a decrease) of ω_1 (ω_2) with x. The frequency shift is a consequence of space- and time-dependent random field which is able to shift either up or down frequencies due to scattering [16, 17].

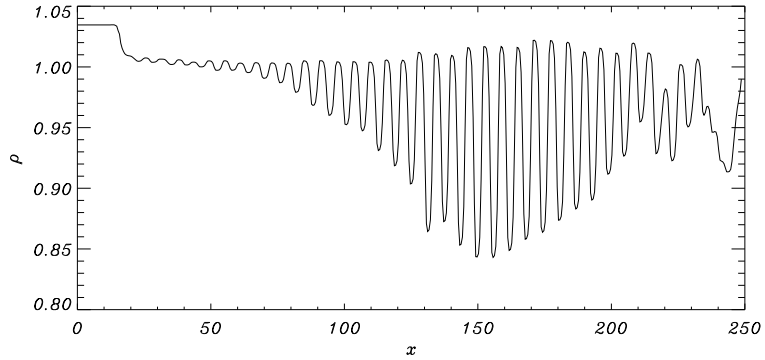

Figure 9. Spatial profiles of the mass density at $t = 20$s and for $y = 25x_0$

To obtain a spectrum for the wavenumber k we proceed as follows. We collect a signal as a function of x at $y_e = 25x_0$ for given time t, $\rho = \rho(x, y = y_e, t)$. An example of such signal for $V_{ey} = 15$m/s is presented in Figure 9.

The corresponding wavenumber, that results from the spectral analysis of such signal, is shown in Figure 10, which reveals that most of the spectral power is centered at $k \cong 1\,\mathrm{m}^{-1}$.

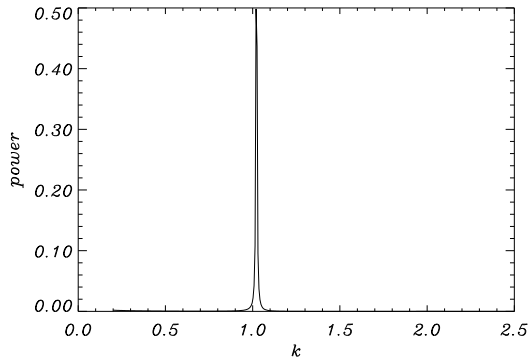

Figure 10. Wavenumber spectrum for the profile of Figure 9

Having determined the frequency ω and the wavenumber k, we compute the phase speed ω/k.

With a use of the results of the above presented analyses, we obtain the speed which is close to the wind speed. However, for the first and second spectral lines the phase speed essentially decreases with x. The strongest decrease is observed for the third spectral line (Figure 11).

5. Summary

In this paper we have developed a numerical model of the transport of air-pollutants in two-dimensional windy atmosphere. The numerical results reveal a number of interesting phenomena such as complex profiles of the pollutants, a plume development and a presence of vortices which result from Kelvin-Helmholtz instabilities.

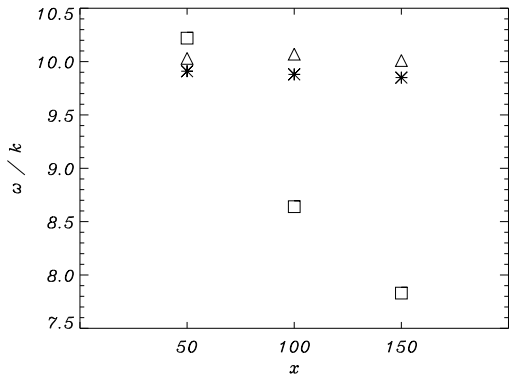

Figure 11. The phase speed that results from the spectral profiles ω and k which are obtained for $x_1 = 50x_0$, $x_2 = 100x_0$, $x_3 = 150x_0$ and for $V_w = 10\,\mathrm{m/s}$. Stars, triangles and squares represent the first, second and third spectral line, respectively

The spatial and temporal profiles have been analysed spectrally to obtain the wavenumber and frequency spectra. The results of this analysis show a frequency shift with the distance from the emittor. The frequency either increases or decreases with the distance x. This shift is a consequence of random scattering.

The random field, that is self-generated by the medium as a result of the interaction between the emission and the horizontal wind, is associated with the mass density, velocity, and pressure as well as it depends on time and space. Such random field enhances spatial spreading of pollutants.

Obviously, the two-dimensional model consists a crude approximation of the three-dimensional atmosphere as in this model the emittor is infinitely wide along the y-direction. However, our approach is justified as it recovers phenomena which would not be resolved accurately, as a consequence of their complexity, in a three-dimensional case which is left for future studies.

Acknowledgements

The authors express their thanks to Dr. Luigi Nocera for his valuable comments to this paper. The numerical computations have been performed in the Poznan Supercomputing and Networking Center. J.K.M.'s work has been financially supported by the State Committee for Scientific Research Grant No. 1039/T07/99/16.

References

[1] Zanetti P 1990 *Air Pollution Modelling: Theories, Computational Methods, and Available Software*, Van Nostrand Reinhold, New York

[2] Bretherton F P and Haidvogel D B 1976 *J. Fluid Mech.* **78** 129

[3] Strużewska J and Łobocki L 1998 *A Comparison of Schemes for Parametrization of the Turbulent Flow in Atmospheric Boundary Layer*, Research Reports of Warsaw University of Technology, Warsaw (in Polish)

[4] Murawski K and Michalczyk J K 2001 *TASK Quarterly* **5** (2) 207

[5] Nieuwstadt F T M and Meeder J P 1997 *Large-eddy Simulation of Air Pollution Dispersion*, Métais O and Fertziger J eds., *New Tools in Turbulence Modelling* Les Editions de Physique, Springer, Kluwer, Paris, pp. 265–279

[6] Straszko J, Fidecka M and Paulo L A 1997 *Protection of the Air and Problems of Waste* **3** 74 (in Polish)

[7] Michalczyk J K and Murawski K 1999 *Protection of the Air and Problems of Waste* **6** 211 (in Polish)
[8] Michalczyk J K, Murawski K and Pawłowski L 1999 *Protection of the Air and Problems of Waste* **2** 50 (in Polish)
[9] LeVeque R J 1997 *CLAWPACK – User Notes*, Applied Mathematics, University of Washington, Seattle, Washington
[10] LeVeque R J 1997 *J. Comput. Phys.* **131** 327
[11] LeVeque R J and Bale D S 1998 *Proc. 7th Int. Conf. on Hyperbolic Problems*, Zurich
[12] Roe P L 1981 *J. Comp. Phys.* **43** 357
[13] LeVeque R J 1998 *J. Comp. Phys.* **146** 346
[14] Rankin R, Harrold B G , Samson J C and Frycz P 1993 *J. Geophys. Res.* **98** 5839
[15] Murawski K, Oliver R and Ballester J L 2001 *Astron. Astrophys.* **375** 264
[16] Murawski K 2000 *Astrophys. J.* **537** 495
[17] Nocera L, Mędrek M and Murawski K 2001 *Astron. Astrophys.* **373** 301